

Cite this: *Mater. Adv.*, 2023,
4, 1583Received 23rd January 2023,
Accepted 15th February 2023

DOI: 10.1039/d3ma00040k

rsc.li/materials-advances

A novel inorganic violet pigment based on zinc niobate

Kazuki Ohnishi,^a Ryohei Oka,^b †*^b Yuga Nomura^a and Toshiyuki Masui †*^c

(Zn_{1-x}Co_x)₃Nb₂O₈ (0 ≤ x ≤ 0.50) samples were synthesized as novel inorganic violet pigments by a conventional solid-state reaction method, and the powders obtained were characterized by using X-ray powder diffraction (XRD), ultraviolet and visible (UV-Vis) diffuse reflectance spectroscopy, and L*a*b*Ch^o chromatic coordinates defined by the Commission Internationale de l'Éclairage (CIE). The (Zn_{1-x}Co_x)₃Nb₂O₈ (0 ≤ x ≤ 0.20) pigments were obtained in a single phase form. The Co atoms introduced into the lattice occupied both octahedral and tetrahedral sites, and the amount of Co in both sites was almost the same. Considering the Laporte rule and the results of the Rietveld analysis, optical absorption was observed around 450 and 530–600 nm in the Co²⁺-doped samples, which was mainly due to the d–d transition of Co²⁺ in the tetrahedral site. The absorption intensity increased with increasing the Co²⁺ concentration. The most vibrant violet color was obtained with (Zn_{0.80}Co_{0.20})₃Nb₂O₈.

Introduction

Inorganic pigments are widely used in a variety of applications such as ceramics, glasses, and cosmetics, because they have high hiding powers and fine coloring properties.^{1–3} Among various colors, violet is known as one of the healing colors to have the effect of relieving tension.⁴ BaCuSi₂O₆ is the first synthesized inorganic violet pigment. This compound absorbs visible light corresponding to yellow-green and shows violet color due to the d–d transition of Cu²⁺ at the square planar tetracoordinate site.^{5,6} But, unfortunately, the chemical stability of BaCuSi₂O₆ is not high enough.⁷ Currently, several violet inorganic pigments are commercially available such as cobalt violet, Co₃(PO₄)₂,^{8–10} and manganese violet, NH₄MnP₂O₇,¹¹ where Co²⁺ and Mn³⁺ are used as the color source, respectively. However, the chroma of these pigments is insufficient. Furthermore, it has been reported that NH₄MnP₂O₇ decomposes at a low temperature of 340 °C.¹¹

When a divalent cobalt ion is used as a color source, unfortunately, the pigment often turns blue, as seen in Co₂SiO₄ olivine,¹² (Co, Zn)₂SiO₄ willemite,¹³ CoAl₂O₄ spinel,¹⁴ and Co₂SnO₄.¹⁵ Against this background, there is a strong demand for new violet inorganic

pigments that are heat resistant and exhibit a bright violet color, and several targeted studies have been conducted.^{7,16,17} In this study, we focused on Zn₃Nb₂O₈ as a host material of novel violet pigment containing Co²⁺ as a color source. This compound has a monoclinic layered structure with a space group of C2/c, consisting of octahedral 6-coordinated Zn²⁺ and Nb⁵⁺, and tetrahedral 4-coordinated Zn²⁺.^{18,19} Zn₃Nb₂O₈ has attracted attention as a magnetic, dielectric, phosphorescent, and photocatalytic material,^{19–23} but has not yet been reported as a pigment. In a pilot experiment, we synthesized Co²⁺-doped Zn₃Nb₂O₈ samples and found that they exhibited a violet color. In this study, therefore, (Zn_{1-x}Co_x)₃Nb₂O₈ (0 ≤ x ≤ 0.50) samples were synthesized and their colors were evaluated. The coordination environment around Co²⁺ was also investigated by crystal structure analysis.

Experimental

Materials and methods

The (Zn_{1-x}Co_x)₃Nb₂O₈ (0 ≤ x ≤ 0.50) samples were synthesized by a conventional solid-state reaction method. ZnO (Kishida Chemical, Japan), Nb₂O₅ (Wako Pure Chemical, Japan) and Co₃O₄ (Wako Pure Chemical, Japan) were used as the starting materials. The raw materials were mixed in a stoichiometric amount and ground in an agate mortar for 30 min. The mixture was calcined in an alumina crucible at 1000 °C for 6 h. The resulting samples were pulverized in an agate mortar before characterization.

Characterization

The sample composition was confirmed by X-ray Fluorescence spectroscopy (XRF: Rigaku, ZSX Primus). The crystal structure

^a Department of Engineering, Graduate School of Sustainability Science, Tottori University, 4-101, Koyama-cho Minami, Tottori 680-8552, Japan

^b Field of Advanced Ceramics, Department of Life Science and Applied Chemistry, Nagoya Institute of Technology, Gokiso, Showa, Nagoya, Aichi 466-8555, Japan. E-mail: oka.ryohei@nitech.ac.jp; Tel: +81-52-735-5365

^c Department of Chemistry and Biotechnology, Faculty of Engineering, and Center for Research on Green Sustainable Chemistry, Tottori University, 4-101, Koyama-cho Minami, Tottori 680-8552, Japan. E-mail: masui@tottori-u.ac.jp; Fax: +81-857-31-5264; Tel: +81-857-31-5264

† R. Oka and T. Masui are co-corresponding authors.



of the sample was identified by X-ray powder diffraction (XRD: Rigaku, Ultima IV) with Cu-K α radiation (40 kV and 40 mA). The XRD data were collected by scanning a 2θ range of 20° to 80° , and the sampling width and the scan speed were 0.02° and $6.0^\circ \text{ min}^{-1}$, respectively. The unit cell volume was calculated with the CellCalc Ver 2.20 software from the refined XRD peak angles using $\alpha\text{-Al}_2\text{O}_3$ as a standard. Rietveld analysis for the XRD patterns obtained in the 2θ range of $10\text{--}120^\circ$ for $(\text{Zn}_{1-x}\text{Co}_x)_3\text{Nb}_2\text{O}_8$ ($x = 0$ and 0.20) was carried out by the RIETAN-FP software package²⁴ to refine the crystal structure and to investigate the site occupancy of Co^{2+} at two non-equivalent Zn^{2+} sites.

The size and morphology of $(\text{Zn}_{1-x}\text{Co}_x)_3\text{Nb}_2\text{O}_8$ ($x = 0, 0.10, 0.15$ and 0.20) were observed using a field-emission-type scanning electron microscope (FE-SEM: JEOL, JSM-6701F). The optical reflectance spectra of the samples were measured with an ultraviolet-visible-near infrared (UV-vis-NIR) spectrometer (JASCO, V-770) with reference to a standard white plate. The color properties of the samples were evaluated on the Commission Internationale de l'Éclairage (CIE) $L^*a^*b^*Ch^\circ$ system using a chroma meter (Konica-Minolta, CR-400), under the following conditions: illuminant C and pulsed xenon lamp as a default light source. This instrument was calibrated with standard calibration plates provided by the manufacturer. The L^* parameter describes the brightness or the darkness of a color with respect to neutral greyscale, while the parameter a^* (the red-green axis) and b^* (the yellow-blue axis) parameters quantitatively describe the color. The chroma parameter (C) represents the color saturation of the pigments, and it is calculated by the following formula: $C = [(a^*)^2 + (b^*)^2]^{1/2}$. The hue angle h° ranges from 0 to 360 , and it is calculated by the formula, $h^\circ = \tan^{-1}(b^*/a^*)$.

Results and discussion

X-ray fluorescence analysis (XRF)

The XRF analysis results of the samples are listed in Table 1. The sample compositions were in good agreement with the nominal stoichiometric compositions of the starting mixtures.

X-ray powder diffraction (XRD) and scanning electron microscopy (SEM)

Fig. 1 shows the XRD patterns of the $(\text{Zn}_{1-x}\text{Co}_x)_3\text{Nb}_2\text{O}_8$ ($0 \leq x \leq 0.50$) pigments. The samples were obtained in a single-

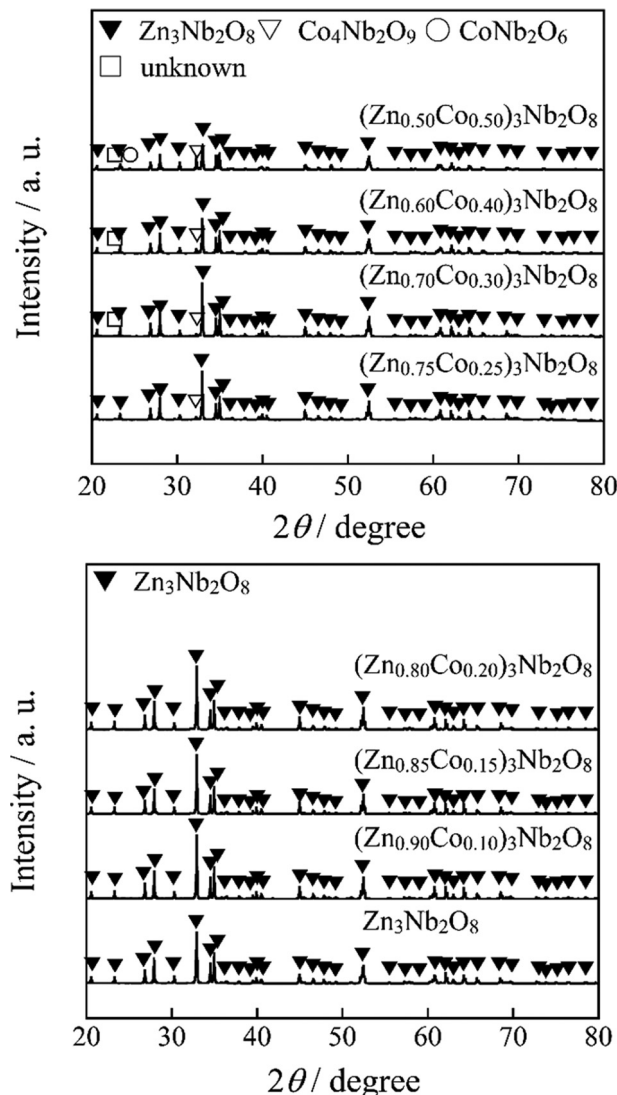


Fig. 1 XRD patterns of the $(\text{Zn}_{1-x}\text{Co}_x)_3\text{Nb}_2\text{O}_8$ ($0 \leq x \leq 0.50$) pigments.

phase form of the monoclinic $\text{Zn}_3\text{Nb}_2\text{O}_8$ phase (space group: $C2/c$) in the range of $0 \leq x \leq 0.20$. However, in the range of $0.25 \leq x \leq 0.50$, $\text{Co}_4\text{Nb}_2\text{O}_9$ and CoNb_2O_6 were observed as impurities, and the sample became a mixed phase. As the Co^{2+} content increased, the diffraction peaks shifted to higher angles. The cell volumes of the $(\text{Zn}_{1-x}\text{Co}_x)_3\text{Nb}_2\text{O}_8$ ($0 \leq x \leq 0.50$) samples calculated from the diffraction angles are summarized in Table 2, where the numbers in parentheses indicate estimated standard deviations.

Since a part of Zn^{2+} (ionic radius: 0.060 nm)²⁵ was replaced with Co^{2+} (ionic radius: 0.058 nm)²⁵, the cell volume monotonically decreased as Co^{2+} increased in the x range of $0 \leq x \leq 0.20$. On the other hand, in the $0.20 \leq x$ region, the degree of lattice shrinkage became smaller than that in the low concentration region. This result indicates that some Co^{2+} ions doped into the samples were not introduced into the lattice, which corresponds to the fact that $\text{Co}_4\text{Nb}_2\text{O}_9$ and CoNb_2O_6 were observed as impurities. Based on the above results, $0 \leq x \leq 0.20$ was the range of the $(\text{Zn}_{1-x}\text{Co}_x)_3\text{Nb}_2\text{O}_8$ solid solutions.

Table 1 Chemical compositions of the $(\text{Zn}_{1-x}\text{Co}_x)_3\text{Nb}_2\text{O}_8$ ($0 \leq x \leq 0.50$) pigments

Stoichiometric composition	Analyzed composition
$\text{Zn}_3\text{Nb}_2\text{O}_8$	$\text{Zn}_{2.93}\text{Nb}_{2.07}\text{O}_{8.11}$
$(\text{Zn}_{0.90}\text{Co}_{0.10})_3\text{Nb}_2\text{O}_8$	$(\text{Zn}_{0.88}\text{Co}_{0.10})_3\text{Nb}_{2.06}\text{O}_{8.09}$
$(\text{Zn}_{0.85}\text{Co}_{0.15})_3\text{Nb}_2\text{O}_8$	$(\text{Zn}_{0.83}\text{Co}_{0.15})_3\text{Nb}_{2.05}\text{O}_{8.07}$
$(\text{Zn}_{0.80}\text{Co}_{0.20})_3\text{Nb}_2\text{O}_8$	$(\text{Zn}_{0.78}\text{Co}_{0.20})_3\text{Nb}_{2.06}\text{O}_{8.09}$
$(\text{Zn}_{0.75}\text{Co}_{0.25})_3\text{Nb}_2\text{O}_8$	$(\text{Zn}_{0.73}\text{Co}_{0.25})_3\text{Nb}_{2.04}\text{O}_{8.07}$
$(\text{Zn}_{0.70}\text{Co}_{0.30})_3\text{Nb}_2\text{O}_8$	$(\text{Zn}_{0.68}\text{Co}_{0.30})_3\text{Nb}_{2.05}\text{O}_{8.07}$
$(\text{Zn}_{0.60}\text{Co}_{0.40})_3\text{Nb}_2\text{O}_8$	$(\text{Zn}_{0.59}\text{Co}_{0.40})_3\text{Nb}_{2.04}\text{O}_{8.07}$
$(\text{Zn}_{0.50}\text{Co}_{0.50})_3\text{Nb}_2\text{O}_8$	$(\text{Zn}_{0.49}\text{Co}_{0.50})_3\text{Nb}_{2.05}\text{O}_{8.10}$



Table 2 Cell volumes of $(\text{Zn}_{1-x}\text{Co}_x)_3\text{Nb}_2\text{O}_8$ ($0 \leq x \leq 0.50$). The numbers in parentheses indicate estimated standard deviations

Sample	Cell volume/nm ³
$\text{Zn}_3\text{Nb}_2\text{O}_8$	0.58333(8)
$(\text{Zn}_{0.90}\text{Co}_{0.10})_3\text{Nb}_2\text{O}_8$	0.58290(6)
$(\text{Zn}_{0.85}\text{Co}_{0.15})_3\text{Nb}_2\text{O}_8$	0.58273(6)
$(\text{Zn}_{0.80}\text{Co}_{0.20})_3\text{Nb}_2\text{O}_8$	0.58238(4)
$(\text{Zn}_{0.75}\text{Co}_{0.25})_3\text{Nb}_2\text{O}_8$	0.58232(11)
$(\text{Zn}_{0.70}\text{Co}_{0.30})_3\text{Nb}_2\text{O}_8$	0.58226(10)
$(\text{Zn}_{0.60}\text{Co}_{0.40})_3\text{Nb}_2\text{O}_8$	0.58215(11)
$(\text{Zn}_{0.50}\text{Co}_{0.50})_3\text{Nb}_2\text{O}_8$	0.5821(2)

Fig. 2 shows the SEM images of $(\text{Zn}_{1-x}\text{Co}_x)_3\text{Nb}_2\text{O}_8$ ($x = 0, 0.10, 0.15$ and 0.20). There was almost no change in the shape and surface condition of the particles, but the particle size slightly increased when Co^{2+} was dissolved into the $\text{Zn}_3\text{Nb}_2\text{O}_8$ lattice. For the Co^{2+} -doped samples, on the other hand, almost no change in the morphologies as well as the particle sizes was observed.

Rietveld analysis

The Rietveld refinements of the XRD patterns recorded for the $(\text{Zn}_{1-x}\text{Co}_x)_3\text{Nb}_2\text{O}_8$ ($x = 0$ and 0.20) samples were performed to estimate the site occupancies of the Co^{2+} ions at the two non-equivalent Zn^{2+} sites. The Rietveld refinement profiles of the samples are shown in Fig. 3, and the crystallographic and structural parameters are summarized in Tables 3 and 4, respectively. The schematic illustration of the $(\text{Zn}_{0.80}\text{Co}_{0.20})_3\text{Nb}_2\text{O}_8$ structure refined by Rietveld analysis is shown in Fig. 4, which was represented by the VESTA program.²⁶ The low R -factors were obtained for both $(\text{Zn}_{1-x}\text{Co}_x)_3\text{Nb}_2\text{O}_8$ ($x = 0$ and 0.20) samples. As illustrated in Fig. 4, there are two non-equivalent Zn^{2+} sites in the lattice and the Zn1 and Zn2 sites are coordinated by six and four O^{2-} ions, respectively. The Rietveld refinement revealed that the Co atoms occupied both octahedral Zn1 and tetrahedral Zn2 sites, as seen in Table 4. The values of multiplicity \times occupancy (g) indicate the amount of the atoms in the unit cell.

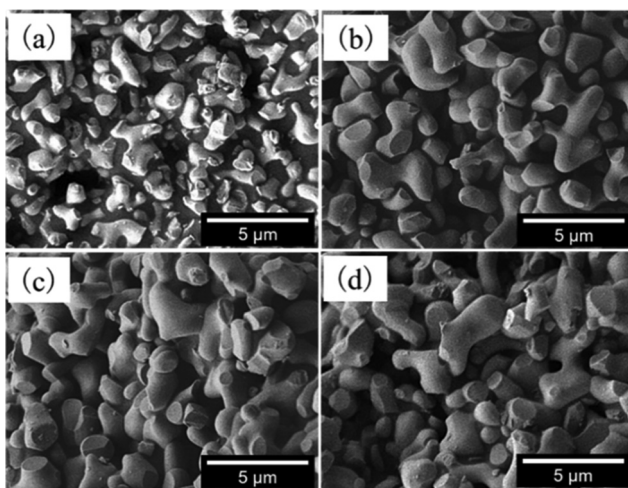


Fig. 2 SEM images of $(\text{Zn}_{1-x}\text{Co}_x)_3\text{Nb}_2\text{O}_8$; $x = 0$ (a), $x = 0.10$ (b), $x = 0.15$ (c), and $x = 0.20$ (d).

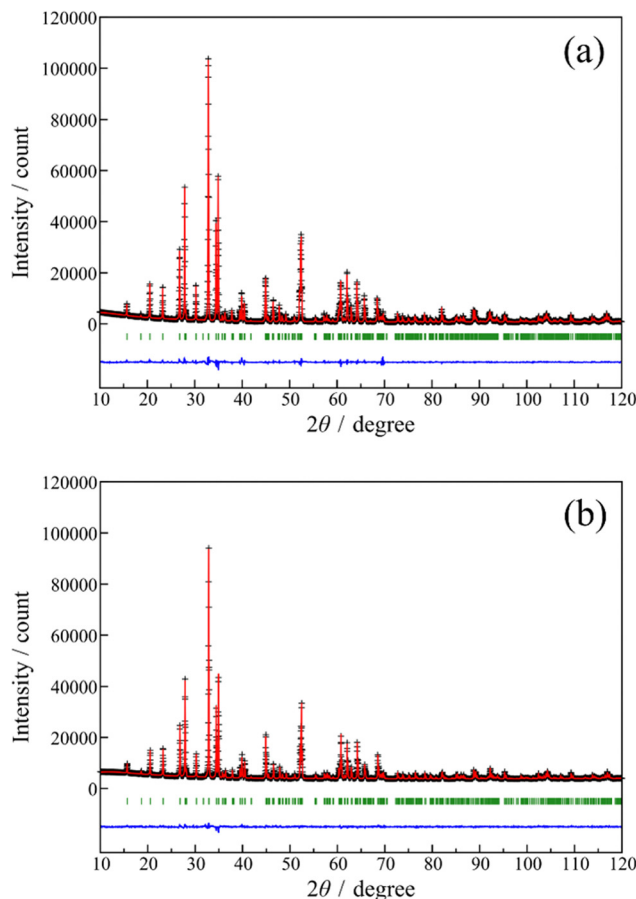


Fig. 3 Rietveld refinement profiles for the $\text{Zn}_3\text{Nb}_2\text{O}_8$ (a) and $(\text{Zn}_{0.80}\text{Co}_{0.20})_3\text{Nb}_2\text{O}_8$ (b) samples. The black cross symbols and the solid red lines represent the observed and calculated intensities, respectively. The difference curves between the observed and calculated patterns are depicted as a blue line at the bottom. The green vertical bars represent the Bragg reflection peak.

Table 3 Crystallographic parameters of the $(\text{Zn}_{1-x}\text{Co}_x)_3\text{Nb}_2\text{O}_8$ ($x = 0$ and 0.20) samples analyzed by the Rietveld refinement^a

	$x = 0$	$x = 0.20$
a/nm	1.90155(2)	1.899061(9)
b/nm	0.590289(5)	0.590063(3)
c/nm	0.519690(4)	0.519720(3)
$\beta/^\circ$	90.0933(5)	89.9923(11)
V/nm^3	0.583333(8)	0.582380(5)
$R_{\text{wp}}/\%$	6.20	1.94
$R_p/\%$	3.99	1.31
$R_c/\%$	2.07	1.41
S	2.99	1.37
$R_f/\%$	2.24	2.56

^a Crystal system: monoclinic, space group: $C2/c$ (No. 15), number of formula units per unit cell: $Z = 4$.

The multiplicity $\times g$ values of the Co atoms at the octahedral (Co1) and tetrahedral (Co2) sites were approximately the same, indicating that the Co atoms did not preferentially occupy only either the octahedral or tetrahedral site. In other words, the Co atoms occupy equally both sites.



Table 4 Structural parameters of the $(\text{Zn}_{1-x}\text{Co}_x)_3\text{Nb}_2\text{O}_8$ ($x = 0$ and 0.20) samples refined by Rietveld analysis

Atom	Site	Occupancy (g)	Multiplicity $\times g$	x	y	z	$B_{\text{iso}}/\text{\AA}^2$
$x = 0$							
Zn1	4e	1	4	0	0.6571(4)	1/4	0.72(3)
Zn2	8f	1	8	0.27863(6)	0.1527(3)	0.2589(4)	$= B_{\text{iso}}(\text{Zn1})$
Nb	8f	1	8	0.11462(5)	0.1636(2)	0.2398(3)	0.53(3)
O1	8f	1	8	0.3197(4)	0.3952(12)	0.4465(12)	0.88(6)
O2	8f	1	8	0.1921(4)	0.3530(13)	0.1299(11)	$= B_{\text{iso}}(\text{O1})$
O3	8f	1	8	0.4287(4)	0.3858(12)	0.0655(13)	$= B_{\text{iso}}(\text{O1})$
O4	8f	1	8	0.0593(3)	0.3723(14)	0.4155(12)	$= B_{\text{iso}}(\text{O1})$
$x = 0.20^a$							
Zn1	4e	0.718 ^b	2.82	0	0.6537(4)	1/4	0.72
Co1	4e	0.282 ^b	1.13	$= x(\text{Zn1})$	$= y(\text{Zn1})$	$= z(\text{Zn1})$	$= B_{\text{iso}}(\text{Zn1})$
Zn2	8f	0.841 ^b	6.72	0.27864(5)	0.1531(3)	0.2554(5)	0.72
Co2	8f	0.159(7)	1.27(6)	$= x(\text{Zn2})$	$= y(\text{Zn2})$	$= z(\text{Zn2})$	$= B_{\text{iso}}(\text{Zn2})$
Nb	8f	1	8	0.11466(4)	0.1634(2)	0.2362(4)	0.53
O1	8f	1	8	0.3209(3)	0.3980(11)	0.4442(11)	0.88
O2	8f	1	8	0.1917(4)	0.3617(12)	0.1320(9)	0.88
O3	8f	1	8	0.4265(3)	0.3873(11)	0.0627(11)	0.88
O4	8f	1	8	0.0606(3)	0.3676(13)	0.4097(11)	0.88

^a The values of the isotropic atomic displacement parameters (B_{iso}) of the zinc, niobium, and oxygen sites for the $(\text{Zn}_{0.80}\text{Co}_{0.20})_3\text{Nb}_2\text{O}_8$ ($x = 0.20$) sample were fixed to them for the $\text{Zn}_3\text{Nb}_2\text{O}_8$ ($x = 0$) sample. The atomic positions and B_{iso} of the Co1 and Co2 sites were constrained to be equal to those of the Zn1 and Zn2 sites. ^b The occupancies of the Zn1, Co1 and Zn2 sites were linearly constrained to be the stoichiometric ratio; $g(\text{Zn1}) = 0.4 + g(\text{Co2})$, $g(\text{Co1}) = 0.6 - g(\text{Co2})$, $g(\text{Zn2}) = 1 - g(\text{Co2})$.

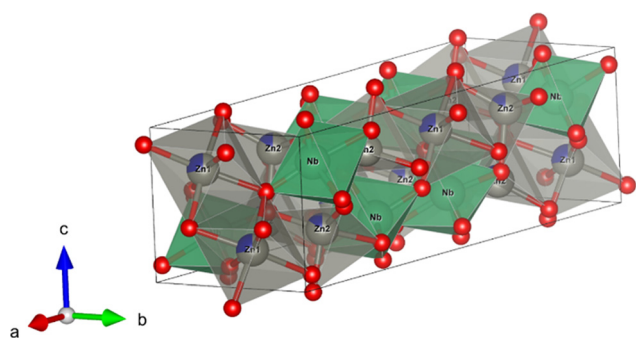


Fig. 4 Crystal structure of $(\text{Zn}_{0.80}\text{Co}_{0.20})_3\text{Nb}_2\text{O}_8$ (gray: Zn, blue: Co, green: Nb, red: O) refined by the Rietveld analysis.

Reflectance and absorbance spectra

The UV-vis reflectance and absorbance spectra of $(\text{Zn}_{1-x}\text{Co}_x)_3\text{Nb}_2\text{O}_8$ ($0 \leq x \leq 0.50$) are shown in Fig. 5. The absorbance spectra were the reflectance spectra that were transformed by using the Kubelka-Munk function, $f(R) = (1 - R)^2/2R$, where R is reflectance.²⁷ The undoped $\text{Zn}_3\text{Nb}_2\text{O}_8$ ($x = 0$) sample exhibited high reflectance in the visible light region. On the other hand, when some Zn^{2+} ions in the lattice were substituted by Co^{2+} ions, optical absorption was observed at wavelengths of 450, 534, 585, and 654 nm. These optical absorption bands were due to the d-d transitions of Co^{2+} , which were mainly tetrahedrally coordinated. As already discussed with respect to the result in Table 4, the Co atoms introduced in the lattice were located at the octahedral and tetrahedral sites and the amount of Co at both sites was almost the same. The octahedral site had parity symmetry while the tetrahedral site did not have an inversion center i . According to the Laporte rule,²⁸ d-d transitions at the former and the latter sites are symmetric forbidden and allowed transitions, respectively. Therefore, the absorption intensities of the

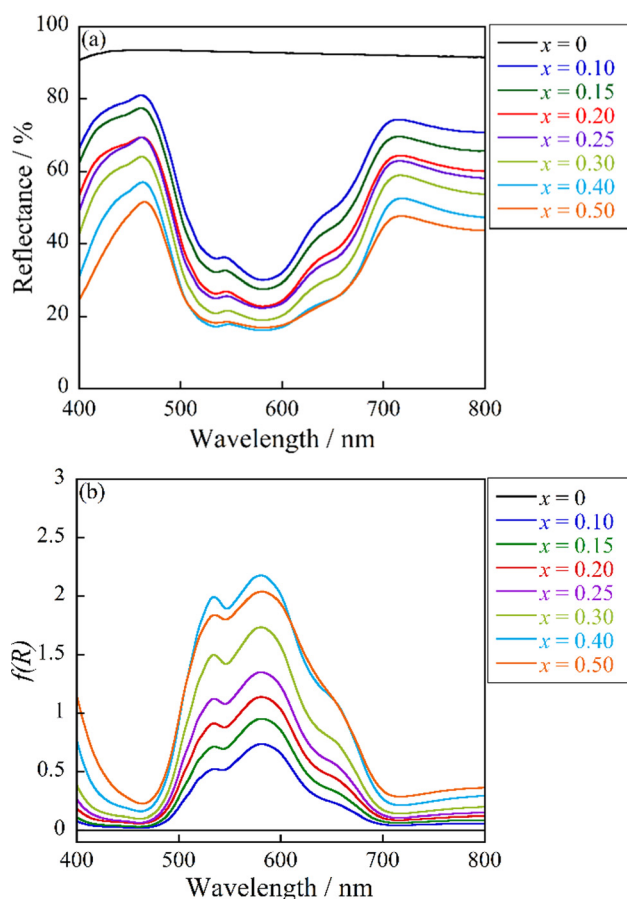


Fig. 5 UV-vis reflectance (a) and absorbance (b) spectra of the $(\text{Zn}_{1-x}\text{Co}_x)_3\text{Nb}_2\text{O}_8$ ($0 \leq x \leq 0.50$) pigments.

d-d transitions of Co^{2+} at the octahedral Zn1/Co1 site could be weaker than those at the tetrahedral Zn2/Co2 site. The main optical



absorption bands for the Co^{2+} -doped samples synthesized in this study could be principally assigned to the d-d transitions of Co^{2+} at the tetrahedral site.

Accordingly, the absorption at 450 nm was attributed to the spin-forbidden transition from ${}^4\text{A}_2({}^4\text{F})$ to ${}^2\text{T}_1({}^2\text{P})$ and the three remaining absorptions at 534, 585, and 654 nm were assigned to the transitions from ${}^4\text{A}_2({}^4\text{F})$ to ${}^2\text{A}_1({}^2\text{G})$, ${}^4\text{T}_1({}^4\text{P})$, and ${}^2\text{E}({}^2\text{G})$, respectively.^{29,30} All these assignments are d-d transitions of Co^{2+} in a tetrahedral coordination, and the contribution of the transition of the octahedral sites was small because of the above-mentioned reasons. The absorption intensity increased with increasing the Co^{2+} concentration.

Chromatic properties

The $L^*a^*b^*Ch^\circ$ color coordinate data for the $(\text{Zn}_{1-x}\text{Co}_x)_3\text{Nb}_2\text{O}_8$ ($0 \leq x \leq 0.50$) pigments are summarized in Table 5. When Co^{2+} was introduced into the host $\text{Zn}_3\text{Nb}_2\text{O}_8$ lattice, the absolute values of both redness (a^*) and blueness ($-b^*$) of the pigment became larger. As seen in Fig. 5, the $(\text{Zn}_{1-x}\text{Co}_x)_3\text{Nb}_2\text{O}_8$ pigments strongly absorbed the green-orange light (500-600 nm) and reflected the blue and red light. As a result, high redness and blueness were obtained, indicating that the Co^{2+} -doped pigments exhibited a violet color. Among the samples synthesized in a single-phase form, $(\text{Zn}_{0.80}\text{Co}_{0.20})_3\text{Nb}_2\text{O}_8$ showed the greatest values ($a^* = +31.4$, $-b^* = 50.1$). The photographs of the $(\text{Zn}_{1-x}\text{Co}_x)_3\text{Nb}_2\text{O}_8$ ($0 \leq x \leq 0.50$) pigments are shown in Fig. 6. The color of the sample changed from white to bright violet with the introduction of Co^{2+} .

Generally, the color tends to be brighter or lighter as the particle size of the pigment decreases.³¹ However, in this study, almost no change in the particle sizes and morphologies was observed for the Co-doped samples, as already discussed above regarding the results of Fig. 2. Accordingly, the color of the $(\text{Zn}_{1-x}\text{Co}_x)_3\text{Nb}_2\text{O}_8$ ($0 \leq x \leq 0.50$) samples depended on the Co^{2+} concentration, directly related to the optical absorption intensity.

Blue color is generally obtained when Co^{2+} is located in a tetrahedral site (e.g., cobalt blue: CoAl_2O_4). In contrast, Co^{2+} at an octahedral site often produces pink or violet (e.g., cobalt violet: $\text{Co}_3(\text{PO}_4)_2$). In this study, the d-d transitions of Co^{2+} at the tetrahedral site were strongly observed, because those at the octahedral and tetrahedral sites were the symmetric forbidden and allowed transitions, respectively, as already discussed in

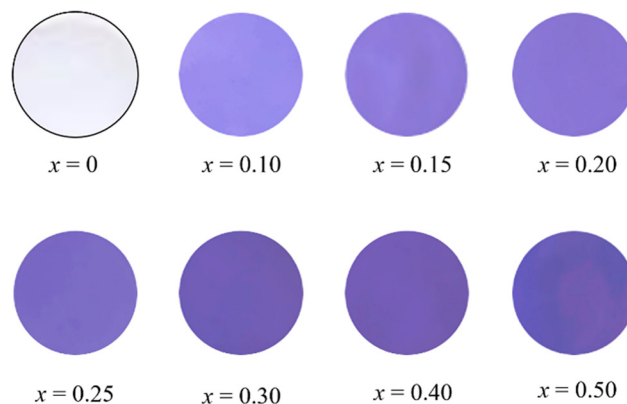


Fig. 6 Photographs of the $(\text{Zn}_{1-x}\text{Co}_x)_3\text{Nb}_2\text{O}_8$ ($0 \leq x \leq 0.50$) pigments.

the previous section. Accordingly, the bluish violet color was obtained for the Co^{2+} -doped samples.

The color coordinate data of the $(\text{Zn}_{0.80}\text{Co}_{0.20})_3\text{Nb}_2\text{O}_8$ sample obtained in a single-phase form were compared with those of the commercially available $\text{Co}_3(\text{PO}_4)_2$ and $\text{NH}_4\text{MnP}_2\text{O}_7$ pigments (Holbein Works, Ltd.), as summarized in Table 6. Although the a^* value of $(\text{Zn}_{0.80}\text{Co}_{0.20})_3\text{Nb}_2\text{O}_8$ was slightly lower than those of commercial pigments, the $-b^*$ and the C values were remarkably higher than those of the commercially available ones.

Chemical stability tests

The chemical stability tests of the $(\text{Zn}_{0.80}\text{Co}_{0.20})_3\text{Nb}_2\text{O}_8$ pigment and the commercially available $\text{Co}_3(\text{PO}_4)_2$ and $\text{NH}_4\text{MnP}_2\text{O}_7$ pigments were evaluated using the powder samples. The acid/base resistance of these pigments was tested in 4% acetic acid and 4% ammonium bicarbonate solutions, and the sample was soaked into the acid/base solutions for 24 h. Then, the sample was washed with deionized water and ethanol, and then dried at room temperature for 24 h. The photographs of the $(\text{Zn}_{0.80}\text{Co}_{0.20})_3\text{Nb}_2\text{O}_8$ pigment and the commercial $\text{Co}_3(\text{PO}_4)_2$ and $\text{NH}_4\text{MnP}_2\text{O}_7$ pigments before/after the chemical stability tests are shown in Fig. 7. The color coordinate values of them before and after the leaching tests are summarized in Table 7. As seen in the photographs of the $(\text{Zn}_{0.80}\text{Co}_{0.20})_3\text{Nb}_2\text{O}_8$ pigment, the color was stable, and no change was observed. Since each value was almost the same before and after the test, the chemical stability of this pigment was quantitatively elucidated. On the other hand, the significant color degradation for the commercial $\text{Co}_3(\text{PO}_4)_2$ and $\text{NH}_4\text{MnP}_2\text{O}_7$ pigments was observed after the acidity and basicity tests, respectively. Therefore, the $(\text{Zn}_{0.80}\text{Co}_{0.20})_3\text{Nb}_2\text{O}_8$ pigment synthesized in this study has good potential to be an alternative to the conventional ones,

Table 5 $L^*a^*b^*Ch^\circ$ color coordinate data for the $(\text{Zn}_{1-x}\text{Co}_x)_3\text{Nb}_2\text{O}_8$ ($0 \leq x \leq 0.50$) pigments

X	L^*	a^*	b^*	C	h°
0	98.7	+0.04	+0.63	0.63	86.4
0.10	65.2	+23.9	-42.5	48.8	299.4
0.15	59.2	+29.4	-48.9	57.1	301.0
0.20	54.3	+31.4	-50.1	59.1	302.1
0.25	52.9	+32.7	-51.6	61.1	302.4
0.30	48.3	+34.8	-53.1	63.5	303.2
0.40	43.3	+35.4	-53.1	63.8	303.7
0.50	39.7	+31.5	-48.6	57.9	302.9

Table 6 The $L^*a^*b^*Ch^\circ$ color coordinates of the $(\text{Zn}_{0.80}\text{Co}_{0.20})_3\text{Nb}_2\text{O}_8$ pigment and commercially available violet pigments

Pigment	L^*	a^*	b^*	C	h°
$(\text{Zn}_{0.80}\text{Co}_{0.20})_3\text{Nb}_2\text{O}_8$	54.3	+31.4	-50.1	59.1	302.1
$\text{Co}_3(\text{PO}_4)_2$	40.7	+42.9	-34.0	54.7	321.6
$\text{NH}_4\text{MnP}_2\text{O}_7$	41.0	+41.8	-27.5	50.0	326.7



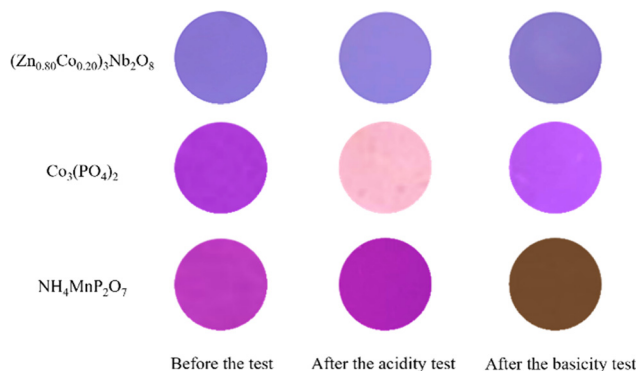


Fig. 7 Photographs of the $(\text{Zn}_{0.80}\text{Co}_{0.20})_3\text{Nb}_2\text{O}_8$ pigment and the commercial $\text{Co}_3(\text{PO}_4)_2$ and $\text{NH}_4\text{MnP}_2\text{O}_7$ pigments before/after chemical stability tests.

Table 7 $L^*a^*b^*Ch^\circ$ color coordinates of the $(\text{Zn}_{0.80}\text{Co}_{0.20})_3\text{Nb}_2\text{O}_8$ pigment and the commercial $\text{Co}_3(\text{PO}_4)_2$ and $\text{NH}_4\text{MnP}_2\text{O}_7$ pigments before and after the chemical stability tests

Pigment	Treatment	L^*	a^*	b^*	C	h°
$(\text{Zn}_{0.80}\text{Co}_{0.20})_3\text{Nb}_2\text{O}_8$	Non-treatment	54.3	+31.4	-50.1	59.1	302.1
	4% CH_3COOH	55.0	+31.1	-49.8	58.7	302.0
	4% NH_4HCO_3	55.3	+30.5	-49.2	57.8	301.8
$\text{Co}_3(\text{PO}_4)_2$	Non-treatment	40.7	+42.9	-34.0	54.7	321.6
	4% CH_3COOH	81.6	+15.1	-4.05	15.6	345.0
	4% NH_4HCO_3	46.1	+38.1	-32.2	49.9	319.8
$\text{NH}_4\text{MnP}_2\text{O}_7$	Non-treatment	41.0	+41.8	-27.5	50.0	326.7
	4% CH_3COOH	41.3	+43.3	-27.1	51.1	327.9
	4% NH_4HCO_3	33.6	+12.5	+19.0	22.8	55.6

because the present pigment has higher chroma (C) and chemical stability than them.

Conclusions

Novel violet inorganic pigments based on $\text{Zn}_3\text{Nb}_2\text{O}_8$ were synthesized by a solid-state reaction method. The color of $\text{Zn}_3\text{Nb}_2\text{O}_8$ changed from white to bright violet when Co^{2+} was doped. The samples were obtained as a single-phase solid solution in the range of $0 \leq x \leq 0.20$ in $(\text{Zn}_{1-x}\text{Co}_x)_3\text{Nb}_2\text{O}_8$, but some impurities were observed in the range of $0.25 \leq x \leq 0.50$. The Rietveld refinement revealed that the Co atoms occupied both octahedral Zn1 and tetrahedral Zn2 sites, and the amount of the Co atoms at octahedral and tetrahedral sites was almost the same. The Co^{2+} -doped samples strongly absorbed visible light from 530 to 600 nm (green to orange light) due to the d-d transition of Co^{2+} and reflected blue and red light. These optical absorption bands were mainly attributed to the d-d transitions of Co^{2+} at the tetrahedral site, considering the Laporte rule and the results of the Rietveld refinement. Among the samples obtained in a single-phase form, $(\text{Zn}_{0.80}\text{Co}_{0.20})_3\text{Nb}_2\text{O}_8$ showed the most vivid violet color, where the $L^*a^*b^*Ch^\circ$ parameters were $L^* = 54.3$, $a^* = +31.4$, $b^* = -50.1$, $C = 59.1$, and $h^\circ = 302.1$. Furthermore, the

$(\text{Zn}_{0.80}\text{Co}_{0.20})_3\text{Nb}_2\text{O}_8$ pigment has higher chemical stability and chroma than the commercial violet pigments. These characteristics indicate that this pigment has good potential to be an alternative to the conventional $\text{Co}_3(\text{PO}_4)_2$ and $\text{NH}_4\text{MnP}_2\text{O}_7$ pigments.

Conflicts of interest

There are no conflicts to declare.

Acknowledgements

This work was supported by JSPS KAKENHI (Grant Numbers JP20H02439 and JP22K04698).

References

- E. B. Faulkner and R. J. Schwartz, *High Performance Pigments*, Wiley-VCH, 2nd edn, 2009.
- K. J. Sreeram, R. Srinivasan, J. M. Devi, B. U. Nair and T. Ramasami, *Dyes Pigm.*, 2007, **75**, 687–692.
- S. Chen, M. Cai and X. Ma, *J. Alloys Compd.*, 2016, **689**, 36–40.
- M. Kido, *J. Intl. Soc. Life Inf. Sci.*, 2000, **18**, 254–268.
- Y. Chen, Y. Zhang and S. Feng, *Dyes Pigm.*, 2014, **105**, 167–173.
- D. A. Corona-Martínez, J. C. Rendón-Angesles, L. A. Gonzalez, Z. Matamoros-Veloz, K. Yanagisawa, A. Tamayo and J. R. Alonso, *Adv. Powder Technol.*, 2019, **30**, 1473–1483.
- P. K. Thejus, B. Koley and K. G. Nishanth, *Dyes Pigm.*, 2018, **158**, 267–276.
- S. Meseguer, M. A. Tena, C. Gargori, J. A. Badenes, M. Llusar and G. Monrós, *Ceram. Int.*, 2007, **33**, 843–849.
- B. Serment, L. Corucho, A. Demourgues, G. HadZioannou, C. Brochon, E. Cloutet and M. Gaudon, *Inorg. Chem.*, 2019, **58**, 7499–7510.
- M. Hunault, J.-L. Robert, M. Newville, L. Galois and G. Calas, *Spectrochim. Acta, Part A*, 2014, **117**, 406–412.
- Y. Begum and A. J. Wright, *J. Mater. Chem.*, 2012, **22**, 21110–21116.
- K. Ullrich, O. Ott, K. Langer and K. D. Becker, *Phys. Chem. Miner.*, 2004, **31**, 247–260.
- L. C. K. de Souza, J. R. Zamian, R. G. N. da Filho, L. E. B. Soledade, I. M. G. dos Santos, A. G. Souza, T. Scheller, R. S. Angélica and C. E. F. da Costa, *Dyes Pigm.*, 2009, **81**, 187–192.
- J. Merikhi, H. O. Jungk and C. Feldmann, *J. Mater. Chem.*, 2000, **10**, 1311–1314.
- A. Shamirian, M. Edrisi and M. Naderi, *J. Mater. Eng. Perform.*, 2013, **22**, 306–311.
- T. Tsukimori, Y. Shobu, R. Oka and T. Masui, *RSC Adv.*, 2018, **8**, 9017–9022.
- S. Tamilarasan, D. Sarma, S. Bhattacharjee, U. V. Waghmare, S. Natarajan and J. Gopalakrishnan, *Inorg. Chem.*, 2013, **52**, 5757–5763.



- 18 T. H. Noh, I.-S. Cho, S. Lee, D. W. Kim, S. Park, S. W. Seo, C. W. Lee and K. S. Hong, *J. Am. Ceram. Soc.*, 2012, **95**, 227–231.
- 19 W.-R. Yang, C.-C. Pan and C.-L. Huang, *J. Alloys Compd.*, 2013, **581**, 257–262.
- 20 L. Li, H. Sun, X. Lv and S. Li, *J. Mater. Sci.: Mater. Electron.*, 2015, **26**, 7026–7031.
- 21 Y. Zhao and P. Zhang, *J. Alloys Compd.*, 2016, **662**, 455–460.
- 22 M.-C. Wu, K.-T. Huang and W.-F. Su, *Mater. Chem. Phys.*, 2006, **98**, 406–409.
- 23 X. Xiao and B. Yan, *Mater. Sci. Eng. B*, 2007, **136**, 154–158.
- 24 F. Izumi and K. Momma, *Solid State Phenom.*, 2007, **130**, 15–20.
- 25 R. D. Shannon, *Acta Crystallogr., Sect. A: Cryst. Phys., Diffraction, Theor. Gen. Crystallogr.*, 1976, **32**, 751–767.
- 26 K. Momma and F. Izumi, *J. Appl. Crystallogr.*, 2011, **44**, 1272–1276.
- 27 P. Kubelka and F. Munk, *Z. Tech. Phys.*, 1931, **12**, 593–601.
- 28 O. Laporte and W. F. Meggers, *J. Opt. Soc. Am.*, 1925, **11**, 459–463.
- 29 M. Ardit, G. Cruciani and M. Donbi, *Am. Mineral.*, 2012, **97**, 1394–1401.
- 30 L. Lin, Y. Wang, B. Lan, J. Chen, S. Lv, Y. Zhao, H. Yu, J. Hao, Q. Zhang, Z. Yang, H. Zhang, J. Wang, J. Qiu and S. Zhou, *J. Phys. Chem. C*, 2019, **123**, 29343–29352.
- 31 S. Ke, Y. Wang and Z. Pan, *Dyes Pigm.*, 2015, **118**, 145–151.

